FUDMA Journal of Sciences (FJS)
ISSN online: 2616-1370
ISSN print: 2645 - 2944
Vol. 10 No. 12, June, 2026, pp 101 – 108
DOI: https://doi.org/10.33003/fjs-2026-1012-5571

Studies on the Adsorption of Cd (II) and Pb (II) Metal ions using Magnetite (Fe_3O_4) Nanoadsorbent from Fertilizer Wastewater

***[1]James Yusuf, [2]Chima Nnachi and [1]Dogara Kantoma**

[1]Department of Applied Chemistry Kaduna Polytechnic, Kaduna State, Nigeria.
[2]Department of Chemistry Federal University Dustin-ma, Katsina State, Nigeria.

*Corresponding authors' email: jamesyusuf@kadunapolytechnic.edu.ng Phone No.: +23489902063

ABSTRACT

The green synthesized nanoadsorbent of magnetite (Fe_3O_4) was characterized for mineralogical phase structure, elemental composition, particles size and morphology. The XRD result showed distinct peaks at angles of 29.20, 33.33, 42.43, 48.22, 58.57, 64.33, 74.44, 76.42 and 86.44 degrees which is related to planes of (102), (104), (110), (113), (204), (116), (214), (300) and (010) with designated phase structure of cubic centered face and crystallite size of 9.04 nm. The elemental compositions also showed a separate peak of iron (Fe, 2.31 keV) and oxygen (O, 0.51 keV). While the surface morphology showed a well dispersed and slightly agglomerated with an average particle size distribution of 15.43 nm as well as dynamic light scattering particle size distribution of 45.76 nm and polydispersity index (PDI) of 0.287. The percentage removal efficiency of Cd(II) metal ions was the highest with 64.43 % when compared with Pb(II) metal ion with 53.43 % in contact time while in adsorbent dose and temperature Pb(II) metal ion had the highest with 68.67% and 65.78 % respectively, in the adsorption process. The kinetic adsorption data fitted well for the pseudo-second-order kinetic model due to the high number of R^2 values of 0.9981and 0.9992 for Cd(II) and Pb(II) metal ions respectively, showing that chemisorption was the rate-determining step. The study demonstrated that magnetite (Fe_3O_4) nanoadsorbent can be utilized in wastewater treatment for the removal of metal ions due to its unique properties.

Received: 07th July 2026

Accepted: 16th July 2026

Published: 28th July 2026

Keywords: Green Synthesis, Nanoadsorbent, Magnetite, Characterization

INTRODUCTION

In recent years, there has been significant research interest in the use of metallic nanoparticles, particularly iron, in the treatment of water pollution (Qasem *et al*., 2021). Where, magnetite (Fe_3O_4) nanoparticles are regarded as one of the most extensively utilized iron-based nanoadsorbents among other phases of iron oxides nanoparticles (Aragaw *et al*., 2021). This is attributed to their exceptionally high surface area to volume ratio and a substantial number of active sites, resulting in a high adsorption affinity and capacity for pollutants compared to many other adsorbents (Xu *et al*., 2024). One of the unique properties of magnetite nanoparticles is that it can be readily separated from the aqueous solution after treatment of wastewater by applying a magnetic field. Additionally, Onyancha *et al*. (2022) reported on the coupling of magnetic separation and ionic exchange of heavy metal ions, which enhances their adsorptive tendency for the removal of heavy metals.

However, adsorption mechanism of pollutants such as heavy metals onto iron oxide surfaces remains a subject of debate. While some researchers have demonstrated that the process is driven by van der Waals interactions (physisorption) with the oxide surface (Qiu *et al*., 2022; Almeida-Naranjo *et al*., 2023), others have proposed chemical reactions involving functional groups chemisorption (Yan *et al*., 2020). Additionally, there are studies suggesting ion exchange between pollutant ions in aqueous solution and iron ions within the lattice structure of iron oxide (Sodzidzi *et al*., 2024). The apparent inconsistencies in the literature can be clarified by considering all factors influencing pollutant removal in the context of the controlling mechanisms (Diener & Mudu, 2021). In an aqueous solution, the surface of iron oxide/hydroxide nanoadsorbents typically undergoes protonation and deprotonation, as indicated by the following reaction (Alnasrawi *et al*., 2023). Hence, this study focused on synthesis of Fe_3O_4 nanoadsorbent derived from green method of synthesis. The synthesized nanoadsorbent was characterized and applied to remove Cd(II) and Pb(II) metal ions from fertilizer wastewater through a batch adsorption process.

MATERIALS AND METHODS

Materials

Sample Collection and Preparation

Collection of Ugu Stem (Telfaira Occidentalis)

The sample of Ugu stem (*Telfaira occidentalis*) plant was collected in Narayi market in Chikun Local Government within Kaduna metropolis. The collected Ugu stem plant was air dried at room temperature for three weeks. Then the dried Ugu stem plant were grinded into a fine powder using motor and pestel. Thirty grams (30 g) of the dried stem powder with 250 mL of ethanol was placed in the soxhlet extractor at 50 C. After six hour of continuous extraction ethanolic stem extract of Ugu plant was obtained. The ethanol content was evaporated using rotary evaporator and the dried extract stored into an air tight container for phytochemical screening.

Collection of Fertilizer Industrial Wastewater

The fertilizer wastewater was randomly collected from from Golden Fertilizer Company along Nnamdi Azikewe Eastern bye pass in Kaduna South Local Government within Kaduna metropolis in morning during dry season. The wastewater sample was collected in clean ten (10) litres polythene plastic container, the sample container was rinsed with the wastewater sample before filling with the sample. The pH of the wastewater sample was measured to be 6.86 at the point of collection and the sample was pretreated with 0.5M HNO_3 for further use.

Methods

Phytochemical screening of Ugu stem (Telfaira occidentalis) leaf extract

Test for Saponins (Foam Test)

In order to confirm the presence of saponins 2 to 3 drops of distilled water was added in 1mL of the extract and there was formation of foam which confirmed the presence of saponins confirmed.

Test for Alkaloids (Wagner Test)

Into a test tube 2 mL of the extract was measured and then 1mL HCl was added. The resulting solution was heated gently for about 20 min and the solution was allowed to cool at room temperature. Finally the resulting solution was filtered and Hager's reagent was added to the filtrate and there was formation of yellow color which confirmed the presence of alkaloids.

Test for Phenol (Ferric Chloride Test)

Into a test tube 2mL of plant extract was measured and four drops of alcoholic ferric chloride ($FeCl_3$) solution was added. The resulting solution turned to bluish black color which confirmed the presence of phenolic compounds.

Test for Terpenoids (Salkowkis)

Into a test tube 5mL of extract was measured and 3mL of chloroform was added. And to the previous solution 3mL of concentrated sulfuric (H_2SO_4) acid was added which turned a reddish brown color which confirmed the presence terpenoids.

Test for Flavonoids

Into a test tube 1mL of the Ugu stem plant extract was measured and a few drops of dilute NaOH solution was added. An intense yellow colour appeared and on addition of few drops of dilute nitric acid the mixture turns to colourless indicating the presence of flavonoids

Test for Tanins

Into a test tube 3 mL of Ugu stem plant extract was measured and diluted with chloroform and 1 mL acetic anhydride was added. Finally 1 mL sulphuric acid was added carefully by the side of the test tube to the mixture a green colour was formed which the presence of tannin

Green Synthesis of Iron Oxide Nanoadsorbent

The synthesis of iron nanoadsorbent was carried out under stirring time of 30 min. 100 cm^3 of precursor mixture of Ferrous Sulphate ($FeSO_4.7H_2O$) and Ferric Chloride ($FeCl_3.6H_2O$) in 1:2 M ratio was measured and transferred into a 250 cm^3 beaker and place on a magnetic stirrer and 10 cm^3 of Ugu (*Telfairia occidentalis*) stem extract was added and the pH of the mixture was adjusted11 using 0.1M NaOH and stirred at 350 rpm and at temperature of 80 °C. The appearance of intense black precipitate was observed which indicates the formation of magnetite Fe_3O_4 nanoadsorbent.

The formed iron nanoparticles was allowed to settle at the bottom of the beaker and the excess liquid was removed by decanting, washed with deionized water severally until the pH of 7 was obtained and dried in an oven at 80 °C for 24h. The obtained nanoparticles was calcined at 500 ^{O}C for 4h in a Murffle furnance (Wen *et al*., 2024).

X – Ray Diffraction (XRD)

The investigation of the phase structure of the synthesized nanoadsorbent of Fe_3O_4 nanoadsorbent was determined by XRD. Each sample was analysed using XRD-7000S Shimadzu coupled with the following measurement conditions, Copper X-ray tube target, 30 kV voltages, 30 mA current, and Kα radiation and the data will be analyzed with PCXRD software. The nanoparticles and nanocomposites respectively will be crushed with agate mortar and pestle, ground to powder form (< 5 µm) and mounted in aluminium plate sample holders with a volume of 0.1 cm^3. The crystalline patterns were compared with the standard line patterns from the powder diffraction file database supplied by International Centre for Diffraction Data (ICDD). The crystallite size was calculated using equation

$$D = \frac{0.9\lambda}{\beta Cos\theta}$$

Where,

D = is the crystallite size

k = 0.9

$\beta =$ is the full width at half maximum (FWHW) of the most intense diffraction plane

λ = is the wavelength of Cu target 1.54 A

θ is the bragg angle

High Resolution Transmission Emission Microscopy (HRTEM)

The morphology and the corresponding selected area electron diffraction (SAED) of the Fe_3O_4 nanoadsorbent was examined by transmission electron microscopy (TEM) and Japan JEOL JEM-1200EX microscope with an accelerating voltage of 80kv, respectively. Small amount of the nanocomposite powders was dispersed in a few milliliters of normal butanol in an ultrasonic bath and sonicated for 30 minutes, and a drop from an eye dropper of this dispersion sample was placed on a copper grid coated with holey carbon film. The samples were placed in a vacuum oven to dry at ambient temperature before examination. The sample was scanned in all zones before the picture was taken.

Determination of Cd (II) and Pb (II) Metal Ions Concentration

The fertilizer wastewater was digested using wet method of digestion. 50 cm^3 of the fertilizer wastewater was measured and transferred into 250 cm^3 beaker and 1:3 ratio of concentrated hydrochloric acid to nitric acid in volume of 5 cm^3 was added. The mixture was heated on a heating mantle at controlled temperature of 80 ^{0}C until the volume reduced to 20 cm^3, then cooled and filtered using Whatman filter paper. The solution was made up to the mark of 100 cm^3, and blank digestion was performed for nitric acid at 80 ^{0}C in the same method. The digestion process was carried out in triplicate and Atomic Absorption Spectrophotometer (AAS) was used to analyse for the metal ions.

Batch Adsorption Experiment

Effect of Contact Time

The effect of various contact time ranging from 15, 30, 45, 60 to 75 min was used to investigate the adsorption of Cd(II) and Pb(II) ions onto Fe_3O_4 nanoadsorbent from the fertilizer wastewater. 50 cm^3 of the fertilizer wastewater was measured and transferred into five different 100 cm^3 conical flasks and corked. The mixture was stirred continuously on a magnetic shaker at 250 rpm under constant condition of pH 6.89, temperature 30 ^{0}C and adsorbent dosage of 0.06 g. The liquid phases were separated from the solution filtration with Whatman filter paper at the end of each mixing period, and the residual concentrations of Cd(II) and Pb(II) metal ions were determined using Atomic Absorption Spectrophotometer (AAS).

Effect of Adsorbent Dosage

The adsorbent dosages ranging from 0.02, 0.04, 0.06, 0.08 to 0.1 g was used to investigate the adsorption of Cd(II) and Pb(II) metal ions onto the Fe_3O_4 nanoadsorbent from the fertilizer wastewater. Exactly 50 cm^3 of the fertilizer wastewater was measured and transferred into five different conical flasks, corked and the mixture was stirred continuously on magnetic stirrer at 250 rpm. All other parameters such as solution pH and constant time were kept constant at 6.89 and 30 min respectively. The liquid phases were separated from the solution filtration with Whatman filter paper at the end of each mixing period, and the residual concentrations of Cd(II) and Pb(II) were determined using Atomic Absorption Spectrophotometer (AAS).

Effect of Temperature

The adsorption of Cd(II) and Pb(II) onto the Fe_3O_4 nanoadsorbent from the fertilizer wastewater was studied at different temperatures 30, 40, 50, and 70 ^{0}C. Exactly 50 cm^3 of the fertilizer wastewater was measured and transferred into five different conical flasks and corked. The mixture was stirred continuously on shaker at 250 rpm regulated by a thermostat attached to a shaker. The solution pH, contact time and adsorbent dosage were kept constant at 6.89, 30 min and 0.03 g respectively. The liquid phases were separated from the solution filtration with Whatman filter paper at the end of each mixing period, and the residual concentrations of Cd(II) and Pb(II) metals were determined using Atomic Absorption Spectrophotometer (AAS).

RESULTS AND DISCUSSION

Phytochemical Screening of Ugu Stem Plant Extracts

The phytochemical screening was carried out to acertain the bioactive compounds qualitatively that will serve as reducing and capping agent in the process of synthesizing the nanoparticles.

Table 1: Result of Phytochemical Screening Of Ugu Stem Plant Extract

Phytochemical compounds	Ugu stem Plant	Name of Test
Alkaloids	+	Wagners
Saponins	+	Foam
Phenols	+	Ferric chloride
Flavonoids	+	Alkaline reagent
Tannins	+	Braymer's
Terpenoids	+	Salkowkis

The confirmatory test, which involved color changes, precipitate formation, and other confirmations, revealed the presence of phytochemicals such as alkaloids, flavonoids, saponins, tannins, terpenoids and phenols in the plant stem extract as shown in Table 4.2, which indicates that the vital phytochemical compounds in the plant are present. These phytochemical compounds has different properties such as reduction, capping and stabilization which can mediate the synthesis of nanoparticles by reducing the metallic precursors through neucleation and growth of the nanoparticles (Bhilkar *et al*., 2023; Adeyemi *et al*., 2022). Similar literatures were reported on the using of others plants in the synthesis of nanoparticles *Eucalyptus globulus* plant extract had bioactive compounds such as saponins, tannins, terpenoids and phenols used in the synthesis of TiO_2 nanoparticles (Harsha *et al*., 2022) . Zarei *et al*. (2020) report bioactive compounds such flavonoids, saponins, tannins, terpenoids and phenols in the plant of *Caralluma tuberculata* extract for the synthesis of Ag_2O nanoparticles. The plant extracts of Moringa oleifera and *Lathyrus sativus* peel extract were used in Fe_3O_4 nanoadsorbent with the presence of bioactive compounds (Dhar *et al*., 2021; Kiwumulo *et al*., 2022)

XRD analysis of F_3O_4 Nanoadsorbent

The mineralogical phases of the F_3O_4 nanoadssorbent synthesized through green method of synthesis by varying stirring time were investigated using XRD and the results are shown in Figure 1

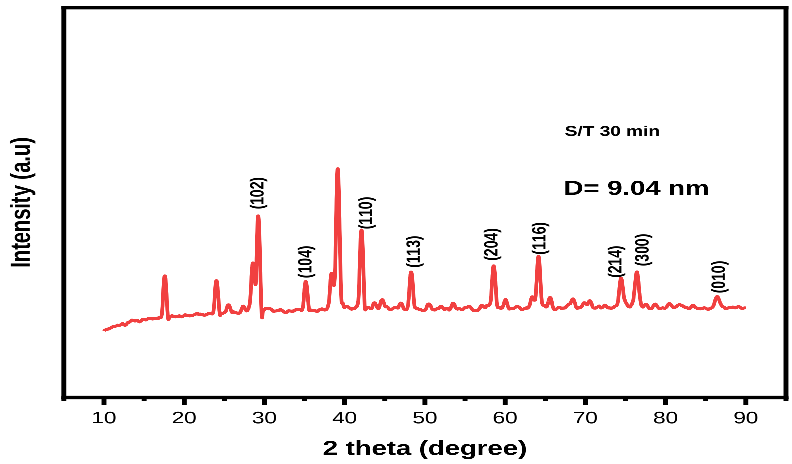

Figure 1: XRD Pattern of Fe_3O_4 Nanoadsorbent Synthesized

The result in Figure 1 shows peaks at 2 theta 29.20, 33.33, 42.43, 48.22, 58.57, 64.33, 74.44, 76.42 and 86.44 degrees related to planes of (102), (104), (110), (113), (204), (116), (214), (300) and (010) which has close agreement with card number of JCPDS 75-1595 and is in agreement with the peaks of magnetite iron nanoparticles synthesized using *Lthyrus sativus* peel extract and *moringa oleifera* plant extract reported by Kiwumulo *et al*. (2022) and Zhu *et al*. (2020).

HRTEM Analysis of Fe_3O_4 Nanoadsorbent

The internal morphologies of the Fe_3O_4 nanoadsorbent synthesized were studied by HRTEM and the results are shown in Figure 2.

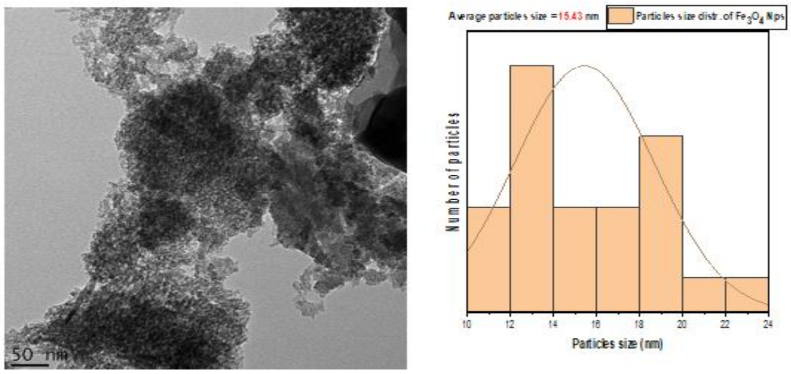

Figure 2: HTEM Image of Synthesized Fe_3O_4 Nanoadsorbent

HRTEM image in plate V (a) of Fe_3O_4 were well dispersed, whereas some of them were slightly agglomerated which could be due to the bioactive compounds of the Ugu stem plant extract or the presence of hydroxyl groups from the plant extract (Joudeh & Linke, 2022). Besides, the tendency of agglomeration is not surprising as the synthesized nanoparticles is high in crystallite size and possesses some magnetic characteristics (Dhar *et al*., 2021). The few large particles found could be due to the agglomeration of smaller particles however, the majority of the particles in the TEM images were 15.43 nm in average particles size.

EDX analysis of Fe_3O_4 nanoadsorbent

The energy dispersive X – ray was used to analyse the elemental composition of the Fe_3O_4 nanoadsorbent and the result is shown in Figure 3.

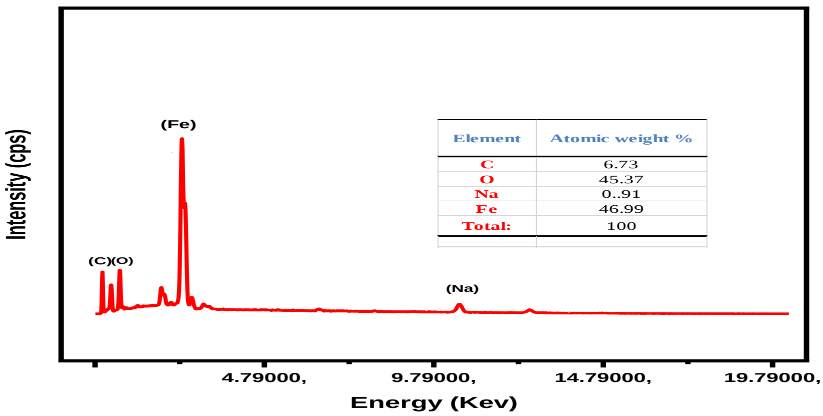

Figure 3: EDX Analysis of Synthesized Fe_3O_4 Nanoadsorbent

The result in Figure 3 show peaks corresponding to C, O, Fe as major elements. Iron has intense peak (Fe, 2.31 keV) and oxygen (O, 0.51 keV) which is in agreement with the studies on *Lathyrus sativus* peel extract and *Calliandra haematocephala* leaf extract reported by Dhar *et al*. (2021) and Kiwumulo *et al*. (2022) other elements such as carbon which might come from the reaction mixture of the synthesized nanoparticles.

DLS Analysis of Fe_3O_4 Nanoadsorbent

The Dynamics Light Scattering (DLS) was used to analyze for the solubility of the Fe_3O_4 nanoadsorbent in aqueous phase and the result is shown in Figure 3.

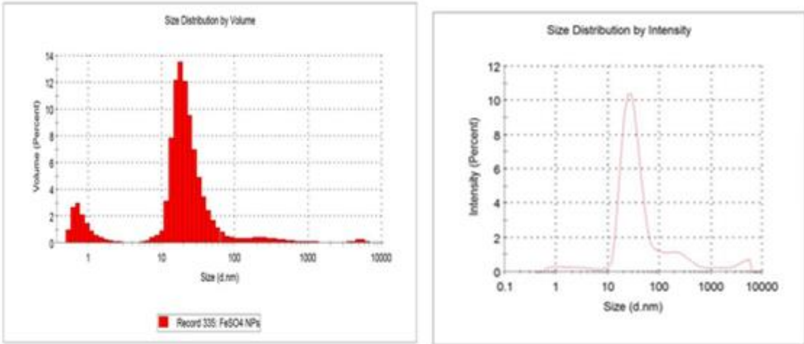

Figure 4: Particles Analysis of Synthesized Fe_3O_4 Nanoadsorbent

The particle size distribution, polydispersity index (PDI), and hydrodynamic diameter of synthesized nanoparticles of Fe_3O_4, was analysed using dynamic light scattering (DLS). The result shows that the particle size distribution was 45.76 nm and the polydispersity index (PDI) was 0.287 and a significant negative zeta potential of −1.7 mV. This negative charge on the developed Fe_3O_4 nanoadsorbent may be due to the various capping agent from the plant sources present on the surface of nanoparticles. In addition the existence of a significant amount of negative charge on the surface of developed nanoparticles, as demonstrated by the high absolute value of zeta potential, would be helpful in the stability of nanoparticles (Mohamed *et al.*, 2023; Ahmed *et al*., 2022).

Heavy Metal Analysis from Fertilizer Wastewater

The results of metal ions concentration from fertilizer wastewater before adsorption shown in table 2 reveals that the concentrations of Cd(II) and Pb(II) metal ions are above the World Health Organization (WHO, 2022) and Nigeria Standard for Drinking Water Quality (NSDWQ, 2023) permissible limit, which pose greater health risk to humans.

Table 2: Heavy Metals Concentration (mg/L) of Cd(II) and Pb(II) from Fertilizer Wastewater Before Adsorption

Parameters (mg/L)	Conc. (mg/L) before adsorption	WHO guideline value (mg/L) - 2022	NSDWQ (mg/L) - 2023
Cadmiun	0.336 ± 0.00	0.03	0.003
Lead	0.564 ± 0.00	0.05	0.1

Batch Adsorption Process

Effect of Contact Time

Contact time is an important parameter because this factor determines the adsorption kinetics of adsorbate at a given initial concentration of the adsorbate. Therefore, the influence of contact time on the adsorption efficiencies of Cd(II) and Pb(II) metal ions from fertilizer wastewater by Fe_3O_4 were studied in the range of 15 -75 minutes and the results are presented in Figure 1.

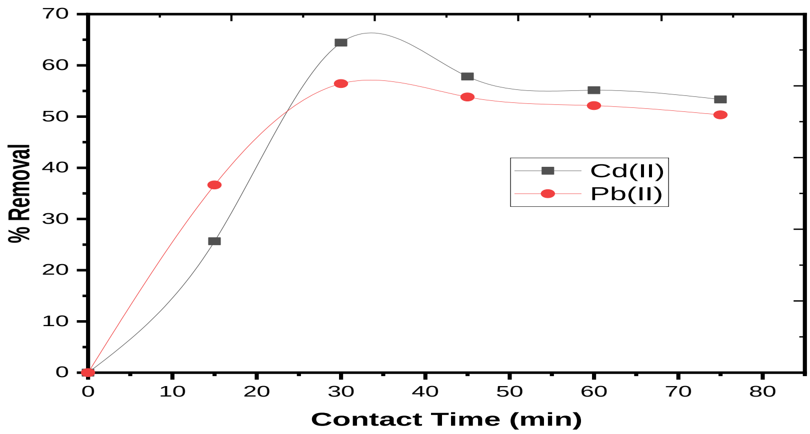

Figure 5: Effect of contact time on the adsorption at pH 6.96, adsorbent dosage (0.06 g) and temperature (30 ◦C)

The percentage adsorption removal of Cd(II) and Pb(II) metal ions by Magnetite (Fe_3O_4) nanoadsorbent is shown in Figure 5. It was discovered that as the contact time between the adsorbent and the wastewater increased, the adsorption efficiency increases rapidly. The optimum time for the removal of Cd(II) and Pb(II) were achieved after 30 min of contact time between the Magnetite (Fe_3O_4) adsorbent and the adsorbate respectively. The result shows that Cd(II) had the highest removal efficiency of 64.43 % when compared with Pb(II) metal ion 53.43 %. The percentage adsorption pattern observed for the heavy metals was in the order of Cd > Pb for the nanoadsorbent which shows the level of affinity to the nanoadsorbent possibly was due to the ionic radius. The observed trend shows that the ionic radius of the heavy metals ions plays an important role in the removal efficacy of the heavy metals. The ionic radius is in the order of Pb(1.91A) > Cd(0.97A). The high percentage removal of Cd(II) mighty be due to diffusion and its removal by the nanoadsorbents which could also be explained according to ionic radius of these metals. Metals with smaller ionic radius would diffuse faster onto the pores of the nanoadsorbents than metal with larger ionic radius.

Effect of Adsorbent Dosage

The adsorbent dose is one of the significant factors that affect the efficiency of adsorbents in the removal of pollutants from wastewater. Adsorbent dosage controls the availability of the binding sites during the adsorption. Thus, the effect of adsorbent dosage (0.02, 0.04, 0.06, 0.08, and 0.1 g) was studied to assess the removal efficiency of Cd(II) and Pb(II) metal ions, from fertilizer wastewater using Fe_3O_4 nanoparticles in Figures 2.

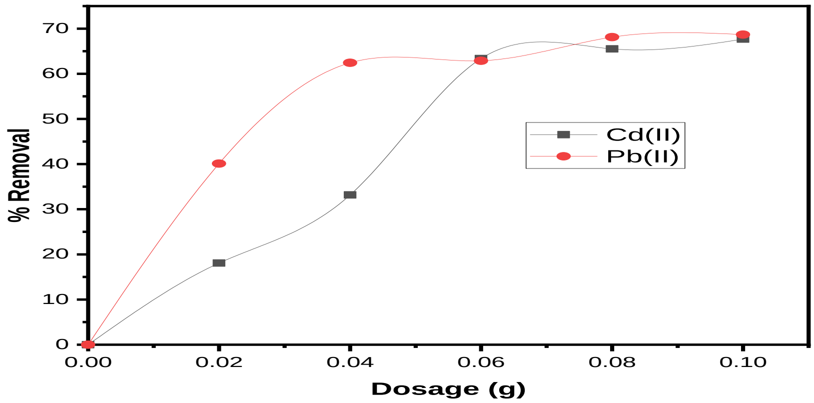

Figure 6: Effect of Adsorbent Dosage on the Adsorption at temperature (30°C) and Contact Time (30 min)

Figure 6 shows that Pb (II) recorded the highest removal efficiency of 68.67% compared to Cd(II) metal ions with 67.68 %, under the conditions of temperature (30℃) and contact time of 30 min. The removal efficiency of the metal ions from fertilizer wastewater exhibited by the nanoadsorbent could be due to its crystallites size and unique properties exhibited by the HRTEM shown in Figure 2 above. It was observed that the removal efficiency was slow between 0.02 to 0.04g and become rapid when the adsorbent increased from 0.04 to 0.06 g. This could be explained in terms of increased coverage of the surface as the adsorbent dosage increases leading to an increase in the number of adsorption sites and enhanced removal efficiency

Effect of Adsorption Temperature

The studies of the adsorption temperature is vital in the adsorption processes (Egbosiuba *et al.*,2021).The effect of different temperatures (30 ℃, 40 ℃, 50 ℃, 60 ℃ and 70 ℃) on the adsorption of Cd(II) and Pb(II) from fertilizer wastewater was carried out and the results are presented in Figure 3.

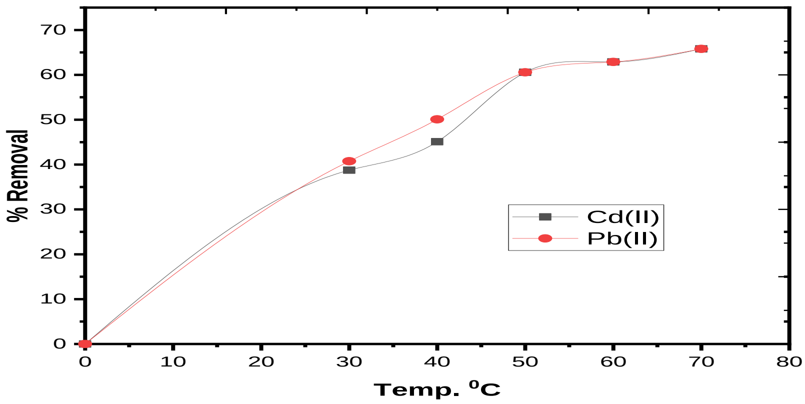

Figure 7: Effect of Temperature on Adsorption removal Cd(II) and Pb(II) at Contact Time of 30 min and dosage (0.03 g)

The percentage adsorption of Cd (II) and Pb (II) metals ions shown in Figure 7 indicates that Cd (II) had the highest percentage removal efficiency compared to Pb (II) metal ions of 65.78 % and 65.18 % respectively. The result suggests that an increase in temperature correspond to increase in the percentage removal of the metals for the nanoadsorbent from the fertilizer wastewater. The increase in removal efficiency as the temperature increases is an indication that temperature plays an important role in the adsorption of Cd(II) and Pb(II) metal ions which suggests that the adsorption process involved chemical reaction as reported by Abdulkareem *et al.* (2023).

Adsorption Kinetics Modelling

Adsorption kinetics is used in order to explain the adsorption mechanism and characteristics of chemical or physical adsorption process as well as the rate constant for batch adsorption. Different kinetic models such as Pseudo-frst order, Pseudo second order, intra-particle diffusion model and Elovich kinetic models were used to study the adsorption that occurs during the removal of Cd (II) and Pb(II) metal ions from fertilizer wastewater using magnetite (Fe_3O_4) nanoadsorbent.

Table 1: Pseudo Order Kinetic Parameters for The Adsorption of Cd (II) and Pb (II) metal ions from Fertilizer Wastewater by Magnetite (Fe_3O_4) Nanoadsorbent

		Magnetite (Fe_3O_4) Nanoadsorbent	
Kinetic models	**Parameters**	**Cd(II)**	**Pb(II)**
Pseudo first order	R^2	0.8111	0.7214
	K_1(1/min)	2.261 x10^{-3}	2.051 x10^{-3}
	q_{eex} (mg/g)	0.0619	0.0518
	qecal (mg/g)	3.699	2.719
	SSE	3.931	2.211
Pseudo second order	R^2	0.9981	0.9992
	K_2(1/min)	0.7819	1.5566
	q_{eex} (mg/g)	0.0609	0.0689
	qecal (mg/g)	2.5020	2.5920
	SSE	0.6451	0.0356
Intraparticle diffusion	R_2	0.9614	0.9766
	K_{id} (1/min)	0.0056	0.0047
	C (mg/g)	2.4612	2.5710
	SSE	1.23 x10^{-5}	1.09x10^{-5}
Elovich	R_2	0.9082	0.9162
	A (1/min)	3.230x10^{-4}	4.23 x10^{-4}
	B (mg/g)	2.4532	2.5282
	SSE	3.45 x10^{-5}	3.87 x10^{-5}

Table 1 above shows the coefficient of correlation values for the pseudo first-order,(R^2) pseudo second order, elovich and intraparticle diffusion kinetic models for the magnetite (Fe_3O_4) nanoadsorbent. The (R^2) value obtained for the pseudo first order kinetic model for the adsorption of Cd (II) and Pb (II) metal ions were found to be 0.8111 and 0.7214 respectively from the fertilizer wastewater which were lower than (R^2) value of pseudo second order kinetic model of 0.9981 and 0.9992. Therefore, pseudo-second- order kinetics demonstrated a significantly better fit of the experimental data in the adsorption phenomena for the metal ions from the fertilizer wastewater onto magnetite Fe_3O_4 nanoadsorbent. This indicate the chemical adsorption of the metal ions onto the homogeneous surface of the nanoadsorbents. The high value of k_2 (0.7819 1/min), (1.5566 1/min) compared to the low values of k_1 (2.051 x10^{-3} 1/min), (2.051 x10^{-3} 1/min) for Cd (II) and Pb(II) metal ions respectively, shows that the adsorption rate of the metal ions from the fertilizer wastewater was faster in pseudo second order than pseudo first order kinetics, also supporting the fact that the reaction fits better into pseudo second order kinetics model. In addition, the pseudo-second-order kinetic model presented the lowest SSE values. Above all, the bond strength between the heavy metals and the nanoadsorbents as well as the active adsorption sites available on the magnetite (Fe_3O_4) nanoadsorbent surface were identified as the determining factor for the rate of metal ions removal from the fertilizer wastewater. Other kinetic models intraparticle diffusion and elovich failed to explain the mechanism of the adsorption of the metal ions by the nanoadsorbent when compared with the pseudo second order (2^{nd}) kinetic models, meaning the adsorption process was not governed by intraparticle diffusion kinetics model and elovich kinetics model due to the lower (R^2) values for Cd (II) and Pb(II) metal ions.

CONCLUSION

The green synthesized magnetite (Fe_3O_4) nanoadsorbent were characterized for mineralogical phase structure, morphology, elemental composition and particle size distribution. The percentage removal efficiency of showed that Cd(II) metal ions had the highest in contact time while the adsorbent dose and temperature Pb(II) metal ion hard the highest in the adsorption process. The kinetic adsorption data fitted well for the pseudo-second-order kinetic model, showing chemisorption as the rate-determining step. The study demonstrated that magnetite (Fe_3O_4) nanoadsorbent has the potential in removal of metals ions from wastewater due to its unique properties.

REFERENCES

Abdulkareem, A. S., Hamzat, W. A., Tijani, J. O., Egbosiuba, T. C., Mustapha, S., Abubakre, O. K., Okafor, B. O., & Babayemi, A. K. (2023). Isotherm, kinetics, thermodynamics and mechanism of metal ions adsorption from electroplating wastewater using treated and functionalized carbon nanotubes. Journal of Environmental Chemical Engineering, 11(1), 109180.

Adeyemi, J. O., Oriola, A. O., Onwudiwe, D. C., & Oyedeji, A. O. (2022). Plant Extracts Mediated Metal-Based Nanoparticles: Synthesis and Biological Applications. Biomolecules, 12(5), 23–40.

Ahmed, S. F., Mofijur, M., Ahmed, B., Mehnaz, T., Mehejabin, F., Maliat, D., Hoang, A. T., & Shafiullah, G. M. (2022). Nanomaterials as a sustainable choice for treating wastewater. Environmental Research, 214(7).

Almeida-Naranjo, C. E., Guerrero, V. H., & Villamar-Ayala, C. A. (2023). Emerging Contaminants and Their Removal from Aqueous Media Using Conventional/Non-Conventional Adsorbents: A Glance at the Relationship between Materials,

Processes, and Technologies. Water (Switzerland), 15(8), 1-7.
Alnasrawi, F. A., Mohammed, A. A., & Tariq, A. M. (2023). Synthesis and application of layered double hydroxides as a superior adsorbent for the removal of hazardous contaminants from aqueous solutions: a comprehensive review. Desalination and Water Treatment, 297, 26–74.

Aragaw, T. A., Bogale, F. M., & Aragaw, B. A. (2021). Iron-based nanoparticles in wastewater treatment: A review on synthesis methods, applications, and removal mechanisms. Journal of Saudi Chemical Society, 25(8), 101280.

Bhilkar, P. R., Bodhne, A. S., Yerpude, S. T., Madankar, R. S., Somkuwar, S. R., Daddemal-Chaudhary, A. R., Lambat, A. P., Desimone, M., Sharma, R., & Chaudhary, R. G. (2023). Phyto-derived metal nanoparticles: Prominent tool for biomedical applications. OpenNano, 14(6), 100192.

Dhar, P. K., Saha, P., Hasan, M. K., Amin, M. K., & Haque, M. R. (2021). Green synthesis of magnetite nanoparticles using Lathyrus sativus peel extract and evaluation of their catalytic activity. Cleaner Engineering and Technology, (3), 100117.

Diener, A., & Mudu, P. (2021). How can vegetation protect us from air pollution? A critical review on green spaces' mitigation abilities for air-borne particles from a public health perspective - with implications for urban planning. Science of the Total Environment, (796) 148605.

Egbosiuba, T.C., Abdulkareem, A.S., Tijani, J.O., Ani, J.I., Krikstolaityte, V., Srinivasan, M., Veksha, A. & Lisak, G (2021). Taguchi optimization design of diameter-controlled synthesis of multi walled carbon nanotubes for the adsorption of Pb(II) and Ni(II) from chemical industry wastewater, Chemosphere, 12(2), 89-93.

Harsha, L., Subramanian, A., Balakrishnan, N., & Prasad, A. (2022). Green Synthesis and Characterization of Titanium Dioxide Nanoparticle (Tio2) Synthesized Using the Leaf of Eucalyptus Globulus – An In Vitro Study. Journal of Complementary Medicine Research, 13(5), 115.

Joudeh, N., & Linke, D. (2022). Nanoparticle classification, physicochemical properties, characterization, and applications: a comprehensive review for biologists. Journal of Nanobiotechnology, 20(1), 1–29.

Kiwumulo, H. F., Muwonge, H., Ibingira, C., Lubwama, M., Kirabira, J. B., & Ssekitoleko, R. T. (2022). Green synthesis and characterization of iron-oxide nanoparticles using Moringa oleifera: a potential protocol for use in low and middle income countries. BMC Research Notes, 15(1), 1–8.

Mohamed, A., Atta, R. R., Kotp, A. A., Abo El-Ela, F. I., Abd El-Raheem, H., Farghali, A., Alkhalifah, D. H. M., Hozzein, W. N., & Mahmoud, R. (2023). Green synthesis and characterization of iron oxide nanoparticles for the removal of heavy metals (Cd2+ and Ni2+) from aqueous solutions with Antimicrobial Investigation. Scientific Reports, 13(1), 1–30.
NSDWQ (2023). Nigerian Standard Industrial. http://rivwarmis.ogunstate. gov.ng/assets/files/Nigerian Standard-for –Drinking Water-Quality-NIS-554-2023 pdf

Onyancha, R. B., Aigbe, U. O., Ukhurebor, K. E., Kusuma, H. S., Darmokoesoemo, H., Osibote, O. A., & Pal, K. (2022). Influence of magnetism-mediated potentialities of recyclable adsorbents for heavy metal ions removal from aqueous solutions – An organized review. Results in Chemistry, 4(4), 100452.

Qasem, N. A. A., Mohammed, R. H., & Lawal, D. U. (2021). Removal of heavy metal ions from wastewater: a comprehensive and critical review. Npj Clean Water, 4(1).

Qiu, M., Liu, L., Ling, Q., Cai, Y., Yu, S., Wang, S., Fu, D., Hu, B., & Wang, X. (2022). Biochar for the removal of contaminants from soil and water: a review. Biochar, 4(1), 1–25.

Sodzidzi, Z., Phiri, Z., Nure, J. F., Msagati, T. A. M., & de Kock, L. A. (2024). Adsorption of Toxic Metals Using Hydrous Ferric Oxide Nanoparticles Embedded in Hybrid Ion-Exchange Resins. Materials, 17(5).

Wen, J., Gao, F., Liu, H., Wang, J., Xiong, T., Yi, H., Zhou, Y., Yu, Q., Zhao, S., & Tang, X. (2024). Metallic nanoparticles synthesized by algae: Synthetic route, action mechanism, and the environmental catalytic applications. Journal of Environmental Chemical Engineering, 12(1), 111742.

WHO (2022). Guidelines for drinking-water quality: fourth edition incorporating the first and second addenda. https://www.who.int/publications/i/item/9789240045064.

Xu, W., Yang, T., Liu, S., Du, L., Chen, Q., Li, X., Dong, J., Zhang, Z., Lu, S., Gong, Y., Zhou, L., Liu, Y., & Tan, X. (2024). Insights into the Synthesis, types and application of iron Nanoparticles: The overlooked significance of environmental effects. Environment International, 15(8).1-8.

Yan, A., Wang, Y., Tan, S. N., Mohd Yusof, M. L., Ghosh, S., & Chen, Z. (2020). Phytoremediation: A Promising Approach for Revegetation of Heavy Metal-Polluted Land. Frontiers in Plant Science, 11(4), 1–15.

Zarei, Z., Razmjoue, D., & Karimi, J. (2020). Green Synthesis of Silver Nanoparticles from Caralluma tuberculata Extract and its Antibacterial Activity. Journal of Inorganic and Organometallic Polymers and Materials, 30(11), 4606–4614.

Zhu, Y., Yang, Q., Lu, T., Qi, W., Zhang, H., Wang, M., Qi, Z., & Chen, W. (2020). Effect of phosphate on the adsorption of antibiotics onto iron oxide minerals: Comparison between tetracycline and ciprofloxacin. Ecotoxicology and Environmental Safety, 205(5), 111345.